Received: 23 August 2019 | Revised: 19 December 2019 | Accepted: 15 January 2020

DOI: 10.1002/ctpp.201900113

Contributions to Plasma Physics

ORIGINAL ARTICLE

Progress with the 5D full-F continuum gyrokinetic code COGENT

Mikhail Dorf | **Milo Dorr**

Lawrence Livermore National Laboratory, Livermore, California,USA

Correspondence
Mikhail Dorf, Lawrence Livermore National Laboratory, Livermore, CA, USA.
Email: dorf1@llnl.gov

Funding information
U.S. Department of Energy, DE-AC52-07NA27344

Abstract

COGENT is an Eulerian gyrokinetic code being developed for edge plasma modelling. The code is distinguished by the use of a high-order finite-volume (conservative) discretization combined with mapped multi-block grid technology. Our recent work is focused on the development of a 5D full-F COGENT version. A numerical algorithm utilizing locally a field-aligned multi-block coordinate system is implemented to facilitate simulations of highly anisotropic microturbulence in the presence of a strong magnetic shear. In this approach, the toroidal direction is divided into blocks such that, within each block, the cells are field-aligned and a non-matching (non-conformal) grid interface is allowed at the block boundaries. Here we report on details of the numerical implementation and present preliminary results of verification studies performed for the case of the ion temperature gradient (ITG) instability in a sheared toroidal annulus geometry.

KEYWORDS

finite-volume methods, gyrokinetics, tokamak edge

1 | INTRODUCTION

Development of full-F computational methods for kinetic plasma transport modelling is of increasing importance in a tokamak edge region where the ion distribution can substantially deviate from a local Maxwellian distribution and therefore the so-called delta-F approximation becomes invalid. Presently, there are two main approaches to solving the kinetic equation: (a) the particle-in-cell (PIC) method, in which macroparticles are used to represent the distribution function, and (b) the continuum (Eulerian) approach, in which the distribution function is represented on a phase-space grid. While PIC methods can facilitate simulations in diverted magnetic field geometries,[1] modelling of low-amplitude edge turbulence subject to an adequate representation of background quasi-equilibrium dynamics may require a very large number of macroparticles to suppress statistical errors in full-F PIC simulations. Therefore, it is of great practical importance to develop continuum (Eulerian) discretization schemes for edge plasma modelling.

Motivated in part by the success of continuum (Eulerian) delta-F codes for core physics, and in part by their potential for high accuracy, the Edge Simulation Laboratory collaboration[2] has been developing a full-F code called COGENT for the edge.[3,4] The code is unique in that it is based on a consistent high-order discretization of the underlying equations, and hence the error (in particular near the X-point) can be bounded. It utilizes multi-block grid technology, in which logically distinct blocks are smoothly mapped from rectangular computational domains, and a high-order interpolation is used to provide data communication between the blocks. The code presently solves the electrostatic

gyrokinetic system in the long-wavelength limit, i.e. assuming $k\rho_i \ll 1$. Here, ρ_i is the ion gyroradius, and k is the characteristic wavelength for electrostatic potential variations. Multi-species gyrokinetic equations can be solved in COGENT with a number of increasingly detailed collision models including the non-linear Fokker–Plank operator.[5] Detailed description of axisymmetric (4D) code capabilities including results of cross-separatrix simulations in realistic single-null geometries can be found in refs 3,6. Our recent work has focused on the development of a 5D version of the COGENT code to model edge plasma turbulence. While we maintain the use of standard coordinate systems (e.g. single-block slab or toroidal) as the mode of operation, a numerical algorithm utilizing a locally field-aligned multi-block coordinate system has been developed to facilitate simulations of highly anisotropic microturbulence in the presence of strong magnetic shear and X-points. In this approach, the toroidal direction is divided into blocks, such that within each block the cells are field-aligned, and a non-matching (non-conformal) grid interface is allowed at the block boundaries. The toroidal angle is playing the role of the "coarse" field-aligned coordinate, whereas the poloidal cross-section, comprised of the radial and poloidal directions, is finely gridded to resolve short-scale perpendicular turbulence structures and to support accurate re-mapping (interpolation) at the block boundaries. Previously, we reported on 5D COGENT simulations of the collisionless (universal) instability in a slab geometry for either a single-block Cartesian[7,8] or multi-block field-aligned[8] coordinate option. Here, the initial results of 5D verification studies performed for the case of the ion temperature gradient (ITG) instability in a sheared toroidal annular geometry are presented.

2 | NUMERICAL MODEL

The simulation model considered in this work solves the long-wavelength limit of a 5D full-F ion gyrokinetic equation written in a conservative form:

$$\frac{\partial(B_\parallel^* f)}{\partial t} + \nabla \cdot (\dot{\mathbf{R}} B_\parallel^* f) + \frac{\partial}{\partial v_\parallel}(\dot{v}_\parallel B_\parallel^* f) = 0, \tag{1}$$

where $f(\mathbf{R}, v_\parallel, \mu)$ denotes the ion gyro-averaged distribution function, ∇ is the gradient with respect to $\mathbf{R}$, and the phase-space guiding-center velocities are given by

$$\dot{\mathbf{R}} = \frac{1}{B_\parallel^*}\left[v_\parallel \mathbf{B}^* + \frac{1}{Z_i e}\mathbf{b} \times (Z_i e \nabla\Phi + \mu \nabla B)\right], \tag{2}$$

$$\dot{v}_\parallel = -\frac{1}{m_i B_\parallel^*}\mathbf{B}^* \cdot (Z_i e \nabla\Phi + \mu \nabla B), \tag{3}$$

where m_i and Z_i are the species mass and charge state, respectively, e is the electron charge, $\Phi(\mathbf{R}, t)$ describes the long-wavelength ($k\rho_i \ll 1$) 3D electrostatic potential variations, $\mathbf{B} = B \cdot \mathbf{b}$ is the magnetic field, with $\mathbf{b}$ denoting the unit vector along the field, $\mathbf{B}^*(\mathbf{R}, v_\parallel) \equiv \mathbf{B} + (m_i/Z_i e) v_\parallel \nabla \times \mathbf{b}$, and $B_\parallel^* = \mathbf{B}^* \cdot \mathbf{b}$. The ion kinetic equation is coupled to the gyro-Poisson equation

$$\nabla_\perp \cdot \left(\frac{m_i n_i}{B^2}\nabla_\perp \Phi\right) = e(n_e - Z_i n_i), \tag{4}$$

where the following linear adiabatic electron response is adopted for the case of a core (closed-field-line) toroidal geometry:

$$n_e = \langle n_{i0} \rangle (1 + e\Phi/T_e - e\langle\Phi\rangle/T_e). \tag{5}$$

In Equation (4), $\nabla_\perp \equiv \nabla - \mathbf{b}(\mathbf{b} \cdot \nabla)$, $n_i = (2\pi/m_i) \int f_i B_\parallel^* dv_\parallel d\mu$ is the ion species gyrocenter density, $\langle n_{i0} \rangle \equiv \langle n_i(t=0) \rangle$ is the flux-surface average of its initial profile, with $\langle \cdot \rangle$ denoting the flux surface average operator, and T_e is the electron temperature, which is assumed to be constant for the present purposes. A zero Dirichlet boundary condition is considered at both radial boundaries for electrostatic potential perturbations, and the initial distribution is used to specify inflow boundary fluxes for an ion distribution function.

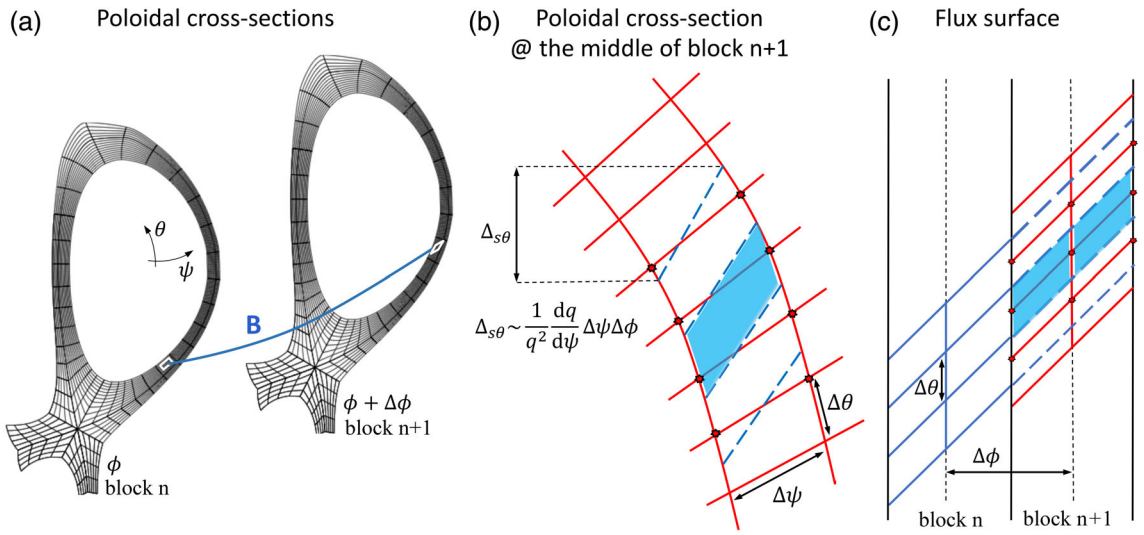

FIGURE 1 Schematic of a locally field-aligned multi-block discretization scheme. Frame (a) shows poloidal cross-sections located in the middle of neighbouring toroidal blocks. Assuming axisymmetric magnetic geometry, the cross-sections are gridded in the same way. Note that the gridding is nearly flux-aligned and has poloidal sub-block structure to deal with the X-point. The control volumes for both valid and ghost cells are obtained in each block by mapping such poloidal grid along the magnetic field lines. A schematic twist and shift of a toroidal face mapped along a magnetic field line is illustrated with two white parallelograms. Frame (b) shows the toroidal faces of block n ghost cells (the blue dashed lines) illustrated over the toroidal faces of block $n+1$ valid cells (the solid red lines). Frame (c) shows an example of the toroidal block structure. In this case, each block has two valid cells (shown with the solid blue and red lines) and two ghost cells. The location of the poloidal planes shown in Frame (a) corresponds to the vertical dashed lines in Frame (c). The shaded blue areas in Frames (b) and (c) illustrate the toroidal and radial faces of the same ghost cell, respectively. The star symbols in Frames (b) and (c) designate the three valid red cells that are used to evaluate the shaded blue ghost cell data for the case of a third-order (quadratic) interpolation.

2.1 | Spatial discretization

COGENT employs high-order finite-volume methods to solve hyperbolic [Equation (1)] and elliptic [Equation (4)] equations on arbitrary spatial grids represented by logically distinct blocks that are smoothly mapped from rectangular computational domains.[4] Short-wavelength turbulence, which determines transport properties of a tokamak plasma, is distinguished by highly anisotropic perturbations that are aligned with the magnetic field, and therefore motivates the use of a field-aligned coordinate system. However, the presence of the X-point and a strong magnetic shear in the edge of a diverted tokamak generates significant distortion of the controlled volumes if a globally field-aligned coordinate system is used. To deal with this issue, the following discretization concept has been adopted (see Figure 1). For the sake of brevity, we leave a detailed description of the numerical algorithm for a future publication and provide only a short summary here.

The toroidal direction is divided into a number of blocks (wedges) such that a local coordinate system is field-aligned within a block. Further, each toroidal block can consist of a number of sub-blocks employed to represent a single-null poloidal cross-section as is done in the 4D (axisymmetric) code.[3,4,6] Assuming axisymmetric equilibrium magnetic geometry, the cell volumes can be constructed within each block in the same way. However, because of the twist and shear of magnetic field lines, the grids in different blocks will not, in general, be conformal. In order to provide communication between the blocks, the grid in each block is extended (along the field lines) into the neighbouring blocks, and the ghost cells thus formed are filled by interpolating the corresponding valid-cell data. Because of the locally field-aligned nature of the discretization scheme, the number of degrees of freedom to describe short-wavelength turbulence remains optimal. That is, while a 2D grid in the poloidal cross-section has to resolve fine-scale structures, e.g. $\lambda \sim \rho_i$, the toroidal direction, which plays the role of a field-aligned coordinate, can remain coarse as it only needs to resolve large-scale parallel structures. We note that some features of the discretization described here are conceptually similar to what is used in ref. 9 for the case of a finite-difference scheme applied to a 3D fluid model. The work in ref. 9, however, considers the case of a flux-independent poloidal coordinate system. Here we emphasize the use of a flux-aligned poloidal grid (with controlled dealignment in the X-point vicinity) in order to be consistent with the 4D transport version and to minimize numerical pollution from the electron physics effects.[3] Finally, we comment on the use of the toroidal angle as a

field-aligned coordinate (as employed here), in contrast to the poloidal angle, which is typically adopted for the modelling of core[10] and edge[11] turbulence. The choice of the poloidal angle as a field-aligned coordinate can be more efficient for modelling high-n modes where it is sufficient to simulate only a small part (wedge) of a full torus. Furthermore, it provides more natural specification of the boundary conditions at the divertor plates. On the other hand, the use of the toroidal angle as a field-aligned coordinate is more natural for X-point modelling where it yields minimal twist of control volumes.

Because of the non-conformity of the toroidal cell faces at the shared block boundaries, special treatment of the inter-block interpolation and the evaluation of normal fluxes at the toroidal block boundaries are required to make the finite-volume scheme globally conservative. While development of a high-order conservative version of the proposed discretization is in progress, we have presently implemented a non-conservative second-order locally field-aligned multi-block version of the code, which can test critical aspects of the numerical scheme. This version utilizes a third-order upwind discretization of the gyrokinetic advection operator combined with a third-order (quadratic) interpolation scheme for the intra-block communication. In the present work we discuss the application of the numerical algorithms to the case of a circular, concentric tokamak configuration

$$\mathbf{B} = \frac{I}{R}\left(\frac{r}{q(r)R_0}\mathbf{e}_\theta + \mathbf{e}_\phi\right), \tag{6}$$

where (r, ϕ, θ) represents the toroidal coordinate system, R is the major radius coordinate, R_0 is the radial distance between the tokamak axis and the core center, and $I = RB_\phi = \text{const}$. Following the analysis in refs 12,13, we define the safety factor profile as $q(r) = q_0 + q_1\exp(q_2\log(r/a))$, where a denotes the minor radius, which is a constant. The locally aligned coordinate system is introduced within each block as follows: the radial coordinate $\xi_0 = r$ labels a flux surface, the field-aligned coordinate $\xi_1 = \phi$ designates the position along a field line as measured by the toroidal angle, and finally the "poloidal" coordinate ξ_2 which labels a field line is defined by $\xi_2 = 2\arctan\left(\frac{1+\bar{r}}{\sqrt{1-\bar{r}^2}}\tan\left(\Theta - \frac{\sqrt{1-\bar{r}^2}}{2}\frac{\phi-\phi_n}{q(\bar{r})}\right)\right)$, where $\bar{r} = r/R_0$, $\Theta = \arctan\left(\frac{\sqrt{1-\bar{r}^2}}{1+\bar{r}}\tan\frac{\theta}{2}\right)$, and ϕ_n designates the reference poloidal plane in block n (here taken as the toroidal centre of a block) where $\xi_2 = \theta$.

2.2 | Field solve

In addition to the spatial discretization described above, developing an efficient approach to solve Equation (4) is necessary. Although a variety of methods are available in COGENT to handle sparsely coupled elliptic equations, the presence of the flux-surface-average potential, which governs the evolution of the axisymmetric (zonal-flow) component, in the RHS of Equation (4) introduces dense (long-range, non-local) coupling. This problem is addressed in COGENT by performing "sub-space" iterations, where we interchangeably solve for flux-surface-averaged (zonal) and non-zonal components of Φ (which belong to orthogonal functional sub-spaces) until the combined solution satisfies the original gyro-Poisson equation. In more detail, introducing $\overline{\Phi} = \langle\Phi\rangle$ and $\widetilde{\Phi} = \Phi - \overline{\Phi}$, we iterate the following system of equations:

$$\nabla_\perp\cdot\left(\frac{m_i n_i}{eB^2}\nabla_\perp\widetilde{\Phi}_{n+1}\right) - \langle n_{i0}\rangle\frac{e\widetilde{\Phi}_{n+1}}{T_e} = \langle n_{i0}\rangle - Z_i n_i - \nabla_\perp\cdot\left(\frac{m_i n_i}{eB^2}\nabla_\perp\overline{\Phi}_n\right), \tag{7}$$

$$\left\langle\nabla_\perp\cdot\left(\frac{m_i n_i}{eB^2}\nabla_\perp\overline{\Phi}_{n+1}\right)\right\rangle = \langle n_{i0}\rangle - \langle Z_i n_i\rangle - \left\langle\nabla_\perp\cdot\left(\frac{m_i n_i}{eB^2}\nabla_\perp\widetilde{\Phi}_{n+1}\right)\right\rangle. \tag{8}$$

Note that Equation (7) for the non-zonal part of Φ does not involve non-local coupling and can be efficiently solved in COGENT by making use of a parallel algebraic multi-grid preconditioner adopted from the Hypre library.[14] The remaining zonal-flow equation [Equation (8)] is a second-order one-dimensional ordinary differential equation that can also be solved straightforwardly. In order to improve the convergence properties of Equations (7)and (8), we subtract the flux-surface-averaged portion of $\widetilde{\Phi}_{n+1}$ each time after solving Equation (7).

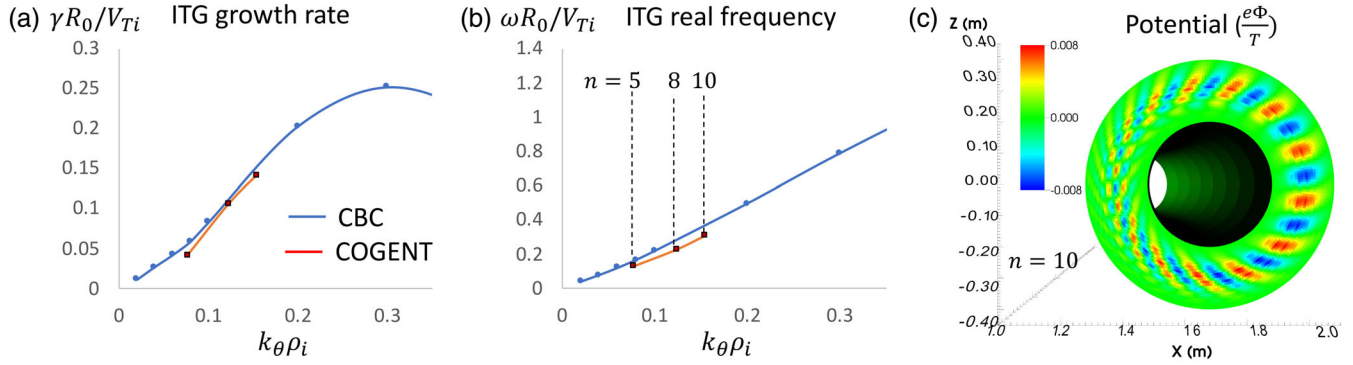

FIGURE 2 Simulations of the CBC test with the single-block toroidal version of COGENT. Frames (a) and (b) illustrate the ITG growth rate and real frequency versus the normalized poloidal wavenumber $k_\theta \rho_i$, respectively, where $k_\theta = nq(r_{\text{mid}})/r_{\text{mid}}$ and n is the toroidal mode number. Global COGENT simulations (red squares) are compared with the results of the local $\rho_i/a \to 0$ model (blue circles). Frame (c) shows the poloidal cross-section of the electrostatic potential variations for the case of $n = 10$.

3 | SIMULATION RESULTS

This section presents the initial results of 5D COGENT verification studies. To test the full-F 5D locally field-aligned multi-block version of the code, the following strategy is adopted. We first benchmark the 5D single-block toroidal version of the code, which employs the standard toroidal coordinate system (r, ϕ, θ), against the linear cyclone base case (CBC) test.[15] Following that verification, the full-F field-aligned version is benchmarked against its single-block toroidal counterpart. Note that direct verification of the field-aligned multi-block version against the CBC results is challenging because of (a) complications with performing toroidal harmonic filtering, as the toroidal coordinate represents a field-aligned coordinate, and (b) pronounced variations in initial electrostatic potential as given by Equations (4) and (5) corresponding to a full-F equilibrium.

3.1 | Single-block toroidal version: cyclone base case test

The results of CBC simulations performed with the single-block toroidal-coordinates (r, ϕ, θ) version of 5D COGENT are shown in Figure 2. The magnetic geometry is given by $R_0 = 1.68$ m, $a = 0.6$ m, $I = RB_\phi = 3.5$ T m, $q_0 = 1.0$, $q_1 = 2.78$, $q_2 = 2.8$ and the radial simulation domain spans $a/3 \le r \le 2a/3$ such that at the middle of the radial domain $r_{mid} = a/2$, $q(r_{mid}) = 1.4$ and $s(r_{\text{mid}}) = (r_{\text{mid}}/q)q'(r_{\text{mid}}) = 0.8$. The singly charged $(Z_i = 1)$ deuterium $(m_i = 2m_p)$ ion species is considered, and the plasma temperature is taken to be $T_e{=}T_i(r_{\text{mid}}){=}$ 2.3 keV, which corresponds to $\rho_i/a \approx 1/180$, where $\rho_i = V_{Ti}/\Omega_i$, $V_{Ti} = \sqrt{T_i/m_i}$, and $\Omega_i = (Z_i e/m_i)(I/R_0)$. Following the verification studies in ref. 16, we take the initial ion distribution as a local Maxwellian distribution with density and temperature profiles specified by the following functional form:

$$A(\psi) = A_0 \left(\frac{\cosh[(\psi - \psi_{\text{mid}} + \delta A)/\Delta A]}{\cosh[(\psi - \psi_{\text{mid}} - \delta A)/\Delta A]} \right)^{-\kappa_A \Delta A/2}, \tag{9}$$

where $\psi = \psi(r)$ is the magnetic flux function which satisfies $\psi' \equiv d\psi/dr = RB_\theta$ subject to a $\psi(0) = 0$ boundary condition, $\psi_{\text{mid}} \equiv \psi(r_{\text{mid}})$, and

$$\kappa_A = \frac{R_0}{L_A} \left[\psi'(r_{\text{mid}}) R_0 \tanh\left(\frac{\delta A}{\Delta A} \right) \right]^{-1}, \tag{10}$$

where $L_A = A/A'(r_{\text{mid}})$ is the inverse logarithmic derivative measured at the middle of the radial domain, and $A' \equiv dA/dr$. The constant parameters in Equations (9) and (10) are given for the initial plasma ion density $(A = N)$ and temperature $(A = T)$ profiles by $R_0/L_N = 2.23$, $R_0/L_T = 6.96$, $T_0 = T_i$, $\delta_N = \delta_T = 2.7 \times 10^{-2}$ T m^2, $\Delta_N = \Delta_T = 4.54 \times 10^{-3}$ T m^2. Results of the COGENT simulations for the toroidal mode numbers $n = 5$, 8, and 10 are shown in Figure 2. This range of toroidal harmonics is chosen to avoid the high-n part of the spectra where the long-wavelength approximation fails and the low-n

part of the spectra where the ITG growth rate is small and requires extended time integration (thereby simulation time). For each simulation, the periodic toroidal domain with the extent of $2\pi/n$ is considered, and all toroidal harmonics higher than the fundamental one are filtered out from the electrostatic potential solution after each solve of Equations (4) and (5). The grid resolution of $[N_\psi = 24, N_\phi = 8, N_\theta = 256, N_{v_\parallel} = 32, N_\mu = 24]$ is adopted for the cases of $n = 8$ and 10, and $N_\theta = 128$ is used for the case of $n = 5$. The velocity domain extent corresponds to $-3.5\sqrt{2T_i/m_i} \le v_\parallel \le 3.5\sqrt{2T_i/m_i}$ and $0 \le \mu \le 8.3T_iR_0/I$. The results of these initial COGENT simulations are found to be in reasonably good agreement with the CBC test results[15] obtained in the local limit, $\rho_i/a \to 0$. The difference can be related to the limited validity of the long-wavelength approximation or the finite orbit width effects due to a finite value ρ_i/a, and will be a subject of our future studies. In conclusion, we note that it takes approximately 1150 CPU-hours (3 min × 384 processors) to simulate a time period of R_0/V_{Ti} (corresponding to 88 time steps) for the case of $n = 5$ on the Cori cluster of the NERSC computing system.[17]

3.2 | Multi-block field-aligned version

In this section we consider simulations of the ITG instability performed with the multi-block field-aligned version of the 5D full-F COGENT code. First, we note that the initial locally Mawellian ion distribution with poloidally uniform density and temperature profiles, which is considered in Section 3.1, corresponds to a steady-state equilibrium only to the zero order in ρ_i/a. As we maintain all toroidal harmonics here, it is important to minimize axisymmetric ($n = 0$) transients during the initial linear stage, and therefore we need to initialize ions with an accurate steady-state distribution. It is also important to note that using a locally Maxwellian distribution as the initial condition yields the development of large-scale ion flows that can interfere with (e.g. delay) the onset of turbulence.[12,18] The guiding-centre equilibrium distribution corresponding to a zero electric field should depend only on the invariants of motion: energy ($E = m_iv_\parallel^2/2 + \mu B$), magnetic moment ($\mu$), and the canonical angular momentum ($P_\phi = Z_ie\psi + m_iv_\parallel RB_\phi/B$). It is evident that a locally Maxwellian distribution function $F_{LM} = N(\psi)[2\pi T(\psi)/m_i]^{-3/2}\exp(m_iv_\parallel^2/2T(\psi) + \mu B/T(\psi))$ can be turned into an equivalent canonical Maxwellian F_{CM} equilibrium function by replacing ψ with

$$\psi_{inv} = \psi + \frac{m_i}{Z_ie}\frac{RB_\phi}{B}v_\parallel, \tag{11}$$

such that in the limit $\rho_i/a \ll 1$ we recover $N(\psi) \approx N(\psi_{\rm inv})$ and $T(\psi) \approx T(\psi_{\rm inv})$. This approach is used here to initialize the ion distribution. Note that a canonical Maxwellian distribution still yields large-scale diamagnetic-size parallel flows. Several authors[12,19] argue that the flows can be minimized by revising the definition of $\psi_{\rm inv}$ in Equation (11) with the use of other constants of motion. The revised expression, however, contains a sign($v_\parallel$) function, which is non-differentiable and was observed to degrade the convergence properties of the attempted test simulations in COGENT. We also point out that sign($v_\parallel$) is not a motion-invariant for trapped particles.

Parameters of the COGENT simulations considered in this section are defined as follows. The magnetic geometry is assumed to be the same as that used in Section 3.1, though a slightly more extended radial domain is considered: 0.19 m $\le r \le$ 0.41 m. The initial plasma profiles are specified by

$$A(\psi_{\rm inv}) = A_0\exp\left[-\kappa_A\Delta A\tanh\left(\frac{\psi_{\rm inv} - \psi_{\rm mid}}{\Delta A}\right)\right], \tag{12}$$

where $\kappa_A = 1/[L_A\psi'(r_{\rm mid})]$. The functional form in Equation (12), which is also used in ref. 12, is adopted here instead of that used in Equation (9), as it is observed to generate less perturbation in plasma profiles when ψ is replaced with $\psi_{\rm inv}$. The initial density and temperature profiles are set by using $R_0/L_N = 5.14$, $R_0/L_T = 16$, $\Delta_N = \Delta_T = 1.8\times10^{-2}$ T m^2.

Following the verification strategy noted earlier (see Section 3), we benchmark the 5D field-aligned multi-block version against its single-block toroidal counterpart (see Figure 3a). For this test simulation we consider a plasma temperature of $T_e{=}T_0 = 7$ keV and a periodic toroidal wedge of $\Delta\phi = 0.2\pi$. The fundamental mode $n = 2\pi/\Delta\phi = 10$ and the associated $k_\theta\rho_i = nq(r_{\rm mid})\rho_i/r_{\rm mid} = 0.27$ correspond to a nearly maximal growth rate in the ITG spectrum. The grid resolution is taken to be $[N_\psi = 48, N_\theta = 256, N_{v_\parallel} = 32, N_\mu = 24]$ and the velocity domain extent is $-3.5\sqrt{2T_i/m_i} \le v_\parallel \le 3.5\sqrt{2T_i/m_i}$ and $0 \le \mu \le 10.4T_iR_0/I$. The multi-block version involves the toroidal domain splitting into two toroidal blocks. Figure 3a shows the time history of the normalized total electrostatic energy corresponding to the non-zonal part of the potential perturbations for the cases of $N_\phi = 8$ and $N_\phi = 16$. The pronounced initial value is due to the fact that the initial canonical

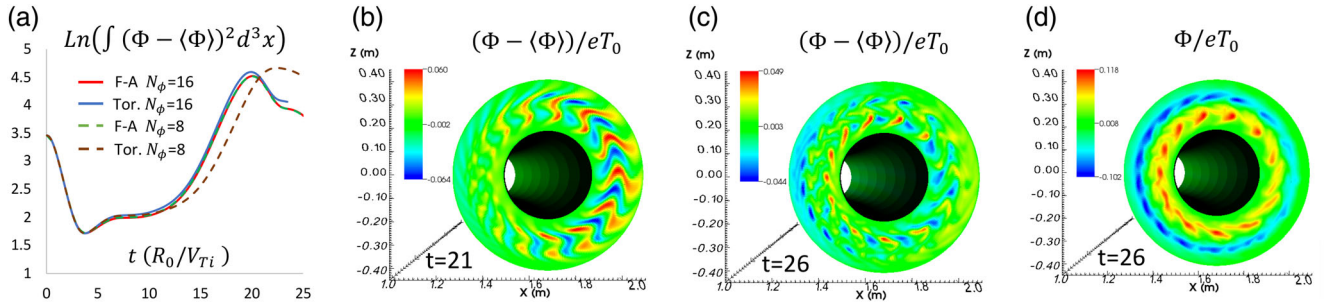

FIGURE 3 Results of the 5D full-F COGENT simulations of the ITG instability in a periodic toroidal wedge $\Delta\phi = 0.2\pi$. Frame (a) shows the total energy of the non-zonal electrostatic perturbations (measured in arbitrary units) obtained with the single-block toroidal (blue and brown curves) and multi-block field-aligned (red and green curves) code versions. The solid curves illustrate the case of $N_\phi = 16$ and the dashed curves correspond to $N_\phi = 8$. The results for potential variations shown in Frames (b–d) are obtained with the multi-block field-aligned code version.

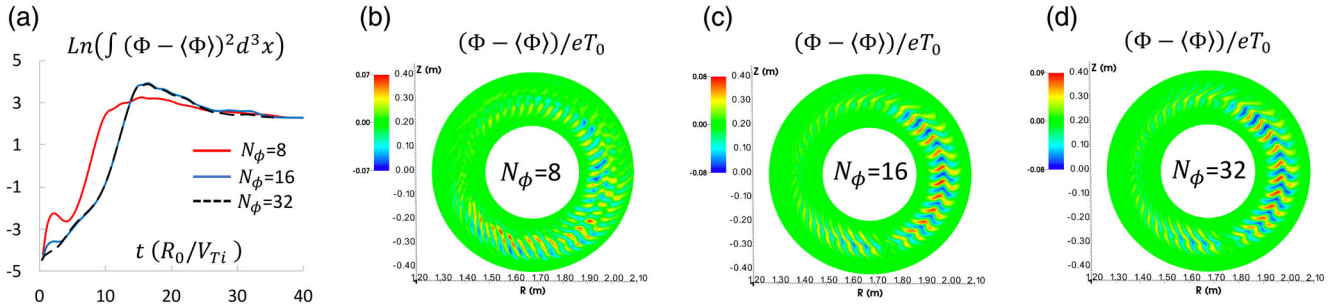

FIGURE 4 Results of the 5D full-F multiblock field-aligned COGENT simulations of the ITG instability in a full torus, $\Delta\phi = 2\pi$. Shown are (a) the time history of the non-zonal electrostatic energy (measured in arbitrary units), and (b–d) poloidal cross-section of non-zonal electrostatic potential perturbations at $t = 15R_0/V_{Ti}$ for different values of the toroidal cell number N_ϕ. The results are obtained with the multi-block version that involves the toroidal domain splitting into two toroidal blocks.

Maxwellian distribution with the plasma profiles in Equation (12) yields poloidal variations in the local ion density, which in turn generates poloidal variations in the electrostatic potential according to Equations (4) and (5). The results obtained with the field-aligned version of the code converge rapidly with respect to the refinement of the toroidal coordinate. The toroidal version appears to produce the same converged result as its field-aligned counterpart, though at a slower convergence rate. Figures 3b–d show the results obtained with the multi-block field-aligned code version. Figures 3b and c plot the non-zonal part of potential perturbations $\Phi - \langle\Phi\rangle$, illustrating evolution of the ITG instability, and Figure 3d shows development of a large-amplitude zonal component $\langle\Phi\rangle$.

Finally, we discuss the results of full-torus, $\Delta\phi = 2\pi$, simulations performed with the multi-block code version that demonstrate the efficiency of the field-aligned discretization (see Figure 4). The parameters of the simulations are the same as those used for Figure 3 except for the plasma temperature $T_0 = T_e = 2.3$ keV and the number of poloidal cells $N_\theta = 340$. Further, in order to observe a pronounced linear stage of the ITG instability, we suppress initial electrostatic potential variations by replacing the adiabatic electron response in Equation (5) with $n_e = n_{i0} + \langle n_{i0}\rangle(e\Phi/T_e - e\langle\Phi\rangle/T_e)$. The results of illustrative simulations performed for different numbers of toroidal cells, $N_\phi = 8$, 16, and 32, show rapid convergence with increase in the resolution of the field-aligned coordinate. This result is consistent with the anisotropic nature of the tokamak micro-turbulence, which is characterized by $k_\perp \sim 1/\rho_i$ and $k_\parallel \sim 1/qR_0$. For the parameters of this simulation, $k_\theta\rho_i \sim 1$ corresponds to the toroidal mode number of $n_{turb} \sim r_{mid}/[q(r_{mid})\rho_i] \approx 65$, which would therefore require 65 times more toroidal points for the equivalent simulation to be performed with the single-block toroidal coordinate code version. In addition to the drastic reduction in the total number of cells, the field-aligned version has much less strict Courant time step constraint for stable explicit integration. Indeed, assuming that N_c cells are needed to adequately resolve a spatial scale, the Courant constraint for the field-aligned code is given by

$\Delta t_{FA} \sim [k_\perp N_c(\rho_i/R_0)V_{Ti}]^{-1} \sim [k_\parallel N_c V_{Ti}]^{-1}$. In contrast, the toroidal code would require $\Delta t_{TC} \sim R_0/(n_{tb} N_c V_{Ti})$, which is about $n_{tb} q \approx 90$ times smaller.

4 | CONCLUSIONS

A locally field-aligned multi-block version of the 5D full-F finite-volume code COGENT is developed. The distinguishing feature of the underlying numerical algorithm is the use of multiple toroidal blocks, such that within each block the cells are field-aligned and a non-matching (non-conformal) grid interface is allowed at the block boundaries. The multi-block approach, together with the use of a toroidal angle as a field-aligned coordinate, can minimize the twist and shear of the field-line-following cells and can facilitate numerical simulations of plasma microturbulence in a divertor (single-null) geometry. In this work, the initial results from 5D simulations of the ITG turbulence in a toroidal annular geometry are presented. The results of the field-aligned multi-block version compare well with those of the single-block toroidal version of COGENT (utilizing the standard toroidal coordinates), while demonstrating significantly enhanced computational efficiency. Our future work will focus on extending the 5D code capabilities to support simulations in a single-null geometry.

ACKNOWLEDGMENTS

The authors are grateful to A. Dimits for fruitful discussions. They also wish to thank their collaborators in the Applied Numerical Algorithms Group, Lawrence Berkeley National Laboratory (LBNL), for their assistance in the development of the numerical algorithms and software infrastructure underlying the COGENT code. This work was supported by the U.S. Department of Energy under contract DE-AC52-07NA27344.

REFERENCES

[1] C. S. Chang, S. Ku, G. R. Tynan, R. Hager, R. M. Churchill, I. Cziegler, M. Greenwald, A. E. Hubbard, J. W. Hughes, *Phys. Rev. Lett.* **2017**, *118*, 175001.
[2] Edge Simulation Laboratory, https://esl.lbl.gov
[3] M. Dorf, M. Dorr, *Contrib. Plasma Phys.* **2018**, *58*, 434.
[4] M. R. Dorr, P. Colella, M. A. Dorf, D. Ghosh, J. A. F. Hittinger, P. O. Schwartz, *J. Comput. Phys.* **2018**, *373*, 605.
[5] M. A. Dorf, R. H. Cohen, M. Dorr, J. Hittinger, T. D. Rognlien, *Contrib. Plasma Phys.* **2014**, *54*, 517.
[6] M. A. Dorf, M. R. Dorr, J. A. Hittinger, R. H. Cohen, T. D. Rognlien, *Phys. Plasmas* **2016**, *23*, 056102.
[7] W. Lee, M. A. Dorf, M. R. Dorr, R. H. Cohen, T. D. Rognlien, J. A. F. Hittinger, M. V. Umansky, S. I. Krasheninnikov, *Contrib. Plasma Phys.* **2018**, *58*, 445.
[8] M. Dorf, M. Dorf, D. Ghosh, J. Hittinger, M.Umansky, J. Angus, IAEA Conf., **2018**.
[9] F. Hariri, M. Ottaviani, *Comput. Phys. Commun.* **2013**, *184*, 2419.
[10] J. Candy, R. E. Waltz, *J. Comput. Phys.* **2003**, *186*, 545.
[11] M. V. Umansky, X. Q. Xu, B. Dudson, L. L. LoDestro, J. R. Myra, *Comput. Phys. Commun.* **2009**, *180*, 887.
[12] V. Grandgirard, Y. Sarazin, X. Garbet, G. Dif-Pradalier, P. Ghendrih, N. Crouseilles, G. Latu, E. Sonnendrücker, N. Besse, P. Bertrand, *Commun. Nonlin. Sci. Numer. Simul.* **2008**, *13*, 81.
[13] V. Grandgirard, J. Abiteboul, J. Bigot, T. Cartier-Michaud, N. Crouseilles, G. Dif-Pradalier, C. Ehrlacher, D. Esteve, X. Garbet, P. Ghendrih, G. Latu, M. Mehrenberger, C. Norscini, C. Passeron, F. Rozar, Y. Sarazin, E. Sonnendrücker, A. Strugarek, D. Zarzoso, *Comput. Phys. Commun.* **2016**, *207*, 35.
[14] Hypre library is a software product of LLNL, CA, USA, http://www.llnl.gov/CASC/hypre/
[15] A. M. Dimits, G. Bateman, M. A. Beer, B. I. Cohen, W. Dorland, G. W. Hammett, C. Kim, J. E. Kinsey, M. Kotschenreuther, A. H. Kritz, L. L. Lao, J. Mandrekas, W. M. Nevins, S. E. Parker, A. J. Redd, D. E. Shumaker, R. Sydora, J. Weiland, *Phys. Plasmas* **2000**, *7*, 969.
[16] G. Merlo, J. Dominski, A. Bhattacharjee, C. S. Chang, F. Jenko, S. Ku, E. Lanti, S. Parker, *Phys. Plasmas* **2018**, *25*, 062308.
[17] National Energy Research Scientific Computing Center. https://nersc.gov
[18] G. Dif-Pradalier, V. Grandgirard, Y. Sarazin, X. Garbet, P. Ghendrih, P. Angelino, *Phys. Plasmas* **2008**, *15*, 042315.
[19] P. Angelino, A. Bottino, R. Hatzky, S. Jolliet, O. Sauter, T. M. Tran, L. Villard, *Phys. Plasmas* **2006**, *13*, 052304.

How to cite this article: Dorf M, Dorr M. Progress with the 5D full-F continuum gyrokinetic code COGENT. *Contributions to Plasma Physics*. 2020;e201900113. https://doi.org/10.1002/ctpp.201900113